

Self-Adaptive Tensor Network States with Multi-Site Correlators

Arseny Kovyrshin and Markus Reiher¹

ETH Zürich, Laboratorium für Physikalische Chemie, Vladimir-Prelog-Weg 2,
8093 Zürich, Switzerland

Abstract

We introduce the concept of self-adaptive tensor network states (SATNS) based on multi-site correlators. The SATNS ansatz gradually extends its variational space incorporating the most important next-order correlators into the ansatz for the wave function. The selection of these correlators is guided by entanglement-entropy measures from quantum information theory. By sequentially introducing variational parameters and adjusting them to the system under study, the SATNS ansatz achieves to keep their number significantly smaller than the total number of full-configuration interaction parameters. The SATNS ansatz is studied for manganocene in its lowest-energy sextet and doublet states, the latter of which is known to be difficult to describe. It is shown that the SATNS parametrization solves the convergence issues found for previous correlator-based tensor network states.

¹Corresponding author: markus.reiher@phys.chem.ethz.ch

1 Introduction

The Density-Matrix Renormalization Group (DMRG)^{1,2} has become a reference approach in the electronic structure theory for problems with strong static electron correlation³⁻¹² such as open-shell transition metal complexes.¹³⁻¹⁷ Its benefit is the polynomial scaling of computational costs due to a tensor-decomposition ansatz instead of the exponential scaling of traditional complete active-space approaches. Originally invented for one-dimensional spin chains¹ with nearest-neighbor interactions, the DMRG optimization algorithm for the full Coulomb problem inherited the one-dimensional order as a sequence of orbitals.

Specifically, DMRG variationally optimizes a matrix product state (MPS) ansatz, a one-dimensional chain of tensors (tensor train).^{18,19} The MPS ansatz allows for a compact description of entanglement in one-dimensional systems. Chemical systems are, however, governed by the full Coulomb interaction producing multidimensional entanglement. In comparison to one-dimensional systems, the convergence of DMRG is slower for chemical systems and a much larger bond-dimension must be taken into account. These problems can be partially alleviated either by employing optimized orbital ordering^{3,20-23} on the sites of the DMRG lattice or by performing an orbital transformation.²⁴

In order to find an optimal wave function ansatz for the representation of multidimensional entanglement, a generalization of the MPS structure was necessary. As a consequence, a new family of wave function parameterizations emerged, the so-called tensor network states (TNS). Examples are the projected entangled pair states (PEPS),²⁵ tree tensor network states (TTNS),^{23,26-31} the multiscale entanglement renormalization ansatz (MERA),³² and the wave function approximation based on the Tucker tensor decomposition.³³

The complete-graph TNS (CGTNS) ansatz³⁴ adopts the correlator product state (CPS) ansatz.³⁵⁻³⁸ The CGTNS ansatz allows all sites to interact with each other on equal footing. However, in its simplest form, it splits the interaction between sites into a product of pair correlators. The number of variational parameters in such a case depends only on the number of spin orbitals and scales as $\mathcal{O}(M^2)$, where M is the number of spin orbitals. But as this ansatz considerably limits the variational degrees of freedom in a fixed fashion, it cannot adjust to a system under study to guarantee a homogeneous error. In our previous work³⁹ we increased the number of variational parameters employing 3-site correlators between sites (spin-orbitals) instead of 2-site

correlators in the original CGTNS ansatz.³⁴ Although the accuracy is then improved, the variational space is inflated, introducing even unnecessary degrees of freedom. In turn, this inflation leads to problems with the optimization of the ansatz.³⁹ Exploiting entanglement measures from quantum information theory,^{21,40,41} we here propose to introduce extra variational freedom only for spin orbitals which are considered more entangled than others. We turn the CGTNS ansatz into a self-adaptive tensor network state (SATNS) ansatz which gradually evolves, guided by entanglement measures. The SATNS ansatz does not introduce all important higher-order correlators at a time but step-wise by starting from most important correlators.

As our SATNS ansatz considers multi-site long-ranged correlators and the full Coulomb interaction, the deterministic optimization⁴² of correlators is not feasible. Hence, for the optimization of correlators, a stochastic approach based on sampling in the discrete Slater determinant space is utilized.³⁴ In this regard the developed method relates to Monte Carlo configuration interaction⁴³ (MCCI), which stochastically searches for important determinants in the full configuration interaction (FCI) space and to the very successful FCI Quantum Monte Carlo.⁴⁴

2 Theory

In this section, we briefly review the original CGTNS ansatz and discuss its variants including higher-order correlators. In Subsection 2.2, the concept of orbital entanglement entropy^{21,40} is introduced for this ansatz. Orbital entropies will play a key role in the extension of the self-adaptive tensor network described in Subsection 2.3. In the last Subsection 2.4, the stochastic optimization of the spin-adapted SATNS wave function is summarized, while a more detailed discussion of this algorithm can be found in Ref. 39.

2.1 Multi-Site Correlator Ansatz

The original CGTNS³⁴ ansatz employs only 2-site correlators, which can be represented by second-order tensors for each pair of spin orbitals i and j

$$\mathbf{C}^{[ij]} \equiv \begin{bmatrix} C_{00}^{[ij]} & C_{01}^{[ij]} \\ C_{10}^{[ij]} & C_{11}^{[ij]} \end{bmatrix}, \quad (1)$$

where the row and column indices n_i and n_j of $C_{n_i n_j}^{[ij]}$ take only two values: 0 for an empty and 1 for an occupied spin orbital. Every 2-site correlator describes the entanglement between a pair of spin orbitals. Multiplying the elements of correlators corresponding to a certain occupation number vector (ONV), one approximates a state of N electrons on M spin orbitals by the 2-site CGTNS ansatz³⁴ of the form

$$|\Psi^{2s}\rangle = \sum_{n_1 n_2 \dots n_M} \prod_{i \leq j} C_{n_i n_j}^{[ij]} |n_1 n_2 \dots n_M\rangle. \quad (2)$$

Eventually $M(M+1)/2$ correlators are used in the CGTNS ansatz, which makes the total number of variational parameters equal to $2M(M+1)$. For complete active space (CAS) -based methods the number of state parameters is defined by the number of ONVs (or configuration state functions for the spin-adapted case). As the active space is defined by the number of electrons, N , and a number of active spatial orbitals, $M_{\text{orb}} = M/2$, we denote it as $\text{CAS}(N, M_{\text{orb}})$. If one considers only ONVs with the spin projection equal to zero and if no symmetry is exploited (not even particle conservation) then the total number of ONVs can be approximated as follows⁴⁵

$$N_{\text{ONV}} \approx \frac{2}{\pi M_{\text{orb}}} 4^{M_{\text{orb}}} = \frac{4}{\pi M} 2^M. \quad (3)$$

For systems with a number of active orbitals of less than eight, the CGTNS ansatz is able to reliably approximate this size of CAS wave function,³⁴ but one will observe severe deviations for systems with larger active spaces. Such deficiencies may be cured by introducing higher-order correlators such as 3-site correlators³⁹ represented by a tensor of third order

$$\mathbf{C}^{[ijk]} \equiv \left[\begin{array}{ccc} & C_{001}^{[ijk]} & \text{---} & C_{011}^{[ijk]} \\ C_{000}^{[ijk]} & \text{---} & C_{010}^{[ijk]} & \text{---} & C_{111}^{[ijk]} \\ & C_{101}^{[ijk]} & \text{---} & C_{110}^{[ijk]} \end{array} \right]. \quad (4)$$

Each of these tensors describes the entanglement between three spin orbitals i , j , and k . Multiplying the elements of these correlators according to the occupations of the ONVs defines the 3-site CGTNS ansatz,

$$|\Psi^{3s}\rangle = \sum_{n_1 n_2 \dots n_M} \prod_{i \leq j \leq k} C_{n_i n_j n_k}^{[ijk]} |n_1 n_2 \dots n_M\rangle. \quad (5)$$

Naturally, such an ansatz achieves a higher accuracy in the energy because of the larger number of variational parameters,³⁹ $M(M+1)(M+2)4/3$ resulting from the 8

elements of the $M(M+1)(M+2)/6$ $\mathbf{C}^{[ijk]}$ correlators. The tedious optimization of 3-site correlators can be enhanced by starting from pre-optimized 2-site correlators in a hybrid ansatz,³⁹ either by optimizing the 3-site correlators as scaling factors,

$$|\Psi^{3s[2s]}\rangle = \sum_{n_1 n_2 \dots n_M} \underbrace{\prod_{i \leq j} C_{n_i n_j}^{[ij]}}_{\text{frozen}} \underbrace{\prod_{k \leq l \leq m} C_{n_k n_l n_m}^{[klm]}}_{\text{active}} |n_1 n_2 \dots n_M\rangle, \quad (6)$$

or preferably by summation of the products of the correlators of different order,

$$|\Psi^{3s+[2s]}\rangle = \sum_{n_1 n_2 \dots n_M} \left[\underbrace{\prod_{i \leq j} C_{n_i n_j}^{[ij]}}_{\text{frozen}} + \underbrace{\prod_{k \leq l \leq m} C_{n_k n_l n_m}^{[klm]}}_{\text{active}} \right] |n_1 n_2 \dots n_M\rangle. \quad (7)$$

Note that the number of variational parameters scales with the highest-order tensor in the expansion. All above-listed parameterization strategies can be naturally continued to higher-order correlators yielding, for instance, Ψ^{4s} , Ψ^{5s} , Ψ^{6s} . Defining the order of correlators by L and recalling from combinatorics that the number of L -combinations with repetitions from a set of size M ^{46,47} one obtains for the number of correlators

$$N_{\text{cor}} = \binom{M+L-1}{L} = \frac{(M+L-1)!}{L!(M-1)!}, \quad (8)$$

while the number of variational parameters is

$$N_{\text{var}} = \left(\frac{(M+L-1)!}{L!(M-1)!} \right) 2^L. \quad (9)$$

For both, M and L , growing, the number of variational parameters exceeds the maximum number of variational parameters defined by traditional CAS-based methods, Eq. (3), unless one limits L to some small value. Therefore, assuming that there are certain ranges for the number of active orbitals, where L is limited to some value, $L \ll M$, one may achieve polynomial scaling, $\mathcal{O}(M^L)$, for the number of variational parameters with system size.

Figure 1: Scaling of the variational parameters with an increasing number of active spatial orbitals M_{orb} in various CGTNS parameterizations (introduced in Sections 2.1 and 2.3) and CAS-based methods. In the blue-shaded region, the CGTNS parameterizations introduce more variational parameters than the exact solution.

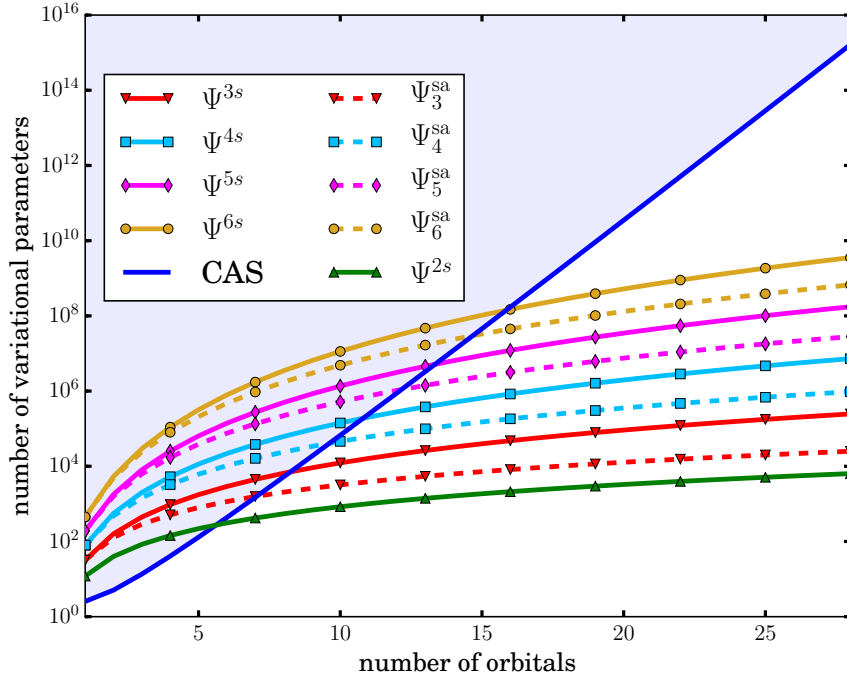


Figure 1 shows the scaling of variational parameters with respect to the number of orbitals for various CGTNS parameterizations and CAS-based methods. However, whereas the 2-site correlators might, for example, already fail to yield an accurate energy, the number of variational parameters introduced in the 3-site correlator ansatz will, in general, be larger than needed, *i.e.*, larger than the one of a traditional CAS ansatz. As a solution to this problem, we suggested to limit the number of higher-order correlators and employ only the most important ones.³⁹We now discuss how orbital entanglement may serve as a criterion for selecting the most important correlators.

2.2 Entanglement Entropy

For the definition of entanglement measures, we bipartition the CGTNS wave function by dividing the set of spin orbitals into an active part $|a\rangle = |a_\alpha a_\beta\rangle$ and an environment

$|e\rangle$ ($e = \{n_1, n_2, \dots, n_M\} \setminus \{a_\alpha, a_\beta\}$)

$$|\Psi^{2s}\rangle = \sum_{a_\alpha \dots e_{M-2}} \prod_{i \leq j}^{\alpha, \beta} C_{a_i a_j}^{[ij]} \prod_k^{\alpha, \beta} \prod_{l=1}^{M-2} C_{a_k e_l}^{[kl]} \prod_{m=1}^{M-2} \prod_{m \leq n} C_{e_m e_n}^{[mn]} |a_\alpha a_\beta e_1 \dots e_{M-2}\rangle. \quad (10)$$

The active part $|a\rangle$ may be one spatial orbital,

$$\{|a\rangle\} = \{|0\rangle, |\text{up}\rangle, |\text{down}\rangle, |2\rangle\}, \quad (11)$$

composed of α - and β -spin orbitals located at the beginning of an ONV. For any other choice of the spatial orbital the resulting bipartition can be transformed into that of Eq. (10) simply by permuting spin orbitals and taking care of sign changes. Introducing weights for each ONV $|ae\rangle = |a_\alpha a_\beta e_1 \dots e_{M-2}\rangle$ as

$$C_{ae}^{2s} = \langle a_\alpha a_\beta e_1 \dots e_{M-2} | \Psi^{2s} \rangle = \prod_{i \leq j}^{\alpha, \beta} C_{a_i a_j}^{[ij]} \prod_k^{\alpha, \beta} \prod_{l=1}^{M-2} C_{a_k e_l}^{[kl]} \prod_{m=1}^{M-2} \prod_{m \leq n} C_{e_m e_n}^{[mn]}, \quad (12)$$

we can rewrite the bipartition in a more convenient way,

$$|\Psi^{2s}\rangle = \sum_{ae} C_{ae}^{2s} |a\rangle |e\rangle. \quad (13)$$

Then, the density operator can be written as

$$\hat{\rho} = \sum_{ae} \sum_{a'e'} C_{ae}^{2s} C_{a'e'}^{2s*} |a\rangle |e\rangle \langle e'| \langle a'|, \quad (14)$$

where we assume real expansion coefficients. After taking the partial trace over the environment, one obtains the reduced one-orbital density operator

$$\hat{\rho}^{(1)} = \text{Tr}_e \hat{\rho} = \sum_e \langle e| \left(\sum_{ae} \sum_{a'e'} C_{ae}^{2s} C_{a'e'}^{2s*} |a\rangle |e\rangle \langle e'| \langle a'| \right) |e\rangle. \quad (15)$$

Recalling the orthonormality of the basis $\{|e\rangle\}$ together with the fact that the number of particles and spin projection are conserved,^{41,48} the expression for the one-orbital reduced density operator can be further simplified

$$\hat{\rho}^{(1)} = \sum_{ae} |C_{ae}^{2s}|^2 |a\rangle \langle a|. \quad (16)$$

Note that these definitions are easily extended to any multi-site CGTNS ansatz. Similar to the Shannon entropy in classical information theory, one can measure the information exchange between active part and environment, which characterizes the entanglement between them, with the von Neumann entropy

$$s_i(1) = -\text{Tr}(\hat{\rho}^{(1)} \ln \hat{\rho}^{(1)}). \quad (17)$$

With a bipartition that puts only one spatial orbital into the active part this entropy is referred to as the single-orbital entropy.^{21,40,41} Since the basis $\{|a\rangle\}$ is orthonormal, the (one-orbital) von Neumann entropy can be expressed as

$$s_i(1) = - \sum_a \omega_a \ln \omega_a, \quad (18)$$

where a runs over the four possible occupations of the spatial orbital (0, up, down, 2) and $\omega_a = \sum_e |C_{ae}^{2s}|^2$. The single-orbital entropy measures the entanglement between orbital a and the remaining set of the orbitals from the active space. In Eq. (10) the correlators of the type $C_{a_\alpha n_i}^{[\alpha i]}$ and $C_{a_\beta n_i}^{[\beta i]}$ for all i (of the environment) are responsible for the information exchange between the orbital a and the rest of the system.⁷ Hence, a high value of single-orbital entropy indicates that one needs to introduce additional variational degrees of freedom in order to better represent the entanglement of the orbital a with the rest of the system. The natural choice is to introduce 3-site correlators of the type $C_{a_\alpha n_i n_j}^{[\alpha ij]}$ and $C_{a_\beta n_i n_j}^{[\beta ij]}$ for all possible i and j , which satisfy the relation $i \leq j$ (all belonging to the environment). In the following, we employ such sets of correlators for an extension of the 2-site CGTNS ansatz. Due to technical reasons these sets also contain the so-called self-interaction³⁹ correlators such as $C_{a_\alpha a_\alpha a_\alpha}^{\alpha \alpha \alpha}$ and $C_{a_\alpha a_\alpha n_j}^{\alpha \alpha j}$.

2.3 Self-Adaptive Tensor Network States

As a set of higher-order correlators might inflate the variational space up to unresolvable degree, it is important to limit them to certain sites selected based on the single-orbital entropies. In our previous work,³⁹ we showed that this efficiently decreases the variational space, simplifies the optimization problem, and yields accurate energies. Here, we suggest a self-adaptive strategy which introduces sets of higher-order correlators described in Section 2.2 sequentially into the CGTNS ansatz. The algorithm at first optimizes the 2-site correlators and then after convergence evaluates single-orbital entropies. Afterwards, the set of 3-site correlators for the spin orbitals α β corresponding to the orbital a with the highest value of the single-orbital entropy is introduced into the ansatz,

$$|\Psi^{\text{sa}}\rangle = \sum_{n_1 \dots n_M} \left[\underbrace{\prod_{i \leq j} C_{n_i n_j}^{[ij]}}_{\text{frozen}} + \underbrace{\prod_{l \leq m} \prod_k^{\alpha, \beta} P(C_{n_k n_l n_m}^{[klm]})}_{\text{active}} \right] |n_1 n_2 \dots n_M\rangle, \quad (19)$$

where the operator P assures the order of the indices k, l, m for correlators according to the following rule (since k is not necessary at the beginning of the ONV)

$$P(C_{n_k n_l n_m}^{[klm]}) = \begin{cases} C_{n_k n_l n_m}^{[klm]}, & \text{if } k \leq l \leq m \\ C_{n_l n_k n_m}^{[klm]}, & \text{if } l \leq k \leq m \\ C_{n_l n_m n_k}^{[klm]}, & \text{if } l \leq m \leq k \end{cases} . \quad (20)$$

Due to the fact that one of the indices (k) of 3-site correlators is forced to take only two values (α and β) the number of 3-site correlators scales similar to the number of 2-site correlators and is equal to

$$N_{\text{cor}} = \left[2 \binom{M+1}{2} - M \right], \quad (21)$$

which yields

$$N_{\text{var}} = \left[2 \binom{M+1}{2} - M \right] 8 \quad (22)$$

3-site variational parameters. Then, after freezing the optimized 3-site correlators, the algorithm automatically introduces correlators for the orbital with the second largest value of the single-orbital entropy, and so forth, generating new sets of correlators until no further decrease of the electronic energy is observed. If, however, 3-site correlators introduced in this way always reduce the electronic energy to a non-negligible degree, 4-site correlator sets can be introduced. If no 3-site correlator set reduces the energy, a 4-site correlator set may be probed to ensure that 2-site correlators are sufficient and can be further optimized.

In the following, the set of correlators being optimized is referred to as the active set, while the associated orbital is called the active orbital. If the SATNS scheme uses correlators up to third order, it will be denoted as Ψ_3^{sa} . One can also extend it with 4- and 5-site correlators and so forth which corresponds to Ψ_4^{sa} , Ψ_5^{sa} , and, ultimately, Ψ_L^{sa} . For the general case, the number of variational parameters is

$$N_{\text{var}} = \left[2 \binom{M+L-2}{L-1} - \binom{M+L-3}{L-2} \right] 2^L. \quad (23)$$

The SATNS introduces and optimizes the higher-order correlators systematically in such a way that the number of variational parameters within the active set of correlators has a similar scaling to that of the previous-order correlator ansatz, $\mathcal{O}(M^{L-1})$, instead of $\mathcal{O}(M^L)$ for all higher-order correlators introduced at once, see Figure 1.

2.4 Optimization Algorithm

Within a given active space and one-particle basis set the expectation value of the electronic Hamiltonian H over the SATNS ansatz can be considered an upper bound to the complete active space configuration interaction (CAS-CI) reference energy,

$$E_{\text{CAS-CI}} = \frac{\langle \Psi_{\text{CAS-CI}} | H | \Psi_{\text{CAS-CI}} \rangle}{\langle \Psi_{\text{CAS-CI}} | \Psi_{\text{CAS-CI}} \rangle} \leq E_{\text{SATNS}} = \frac{\langle \Psi_L^{\text{sa}} | H | \Psi_L^{\text{sa}} \rangle}{\langle \Psi_L^{\text{sa}} | \Psi_L^{\text{sa}} \rangle}. \quad (24)$$

For a spin-adapted CAS-CI wave function a linear expansion of spin-adapted configuration state functions (CSFs), $|\Phi_p^{\text{CSF}}\rangle$, is employed

$$|\Psi_{\text{CAS-CI}}\rangle = \sum_p S_p |\Phi_p^{\text{CSF}}\rangle = \sum_p S_p \sum_n K_{pn} |n\rangle, \quad (25)$$

where K_{pn} are Clebsch–Gordan coefficients. Following our previous work,³⁹ we approximate in the spin-adapted SATNS S_p as follows

$$S_p \approx S_p(\tilde{\mathbf{C}}) = \sum_n K_{pn} C_n^{\text{sa}}, \quad (26)$$

where $C_n^{\text{sa}} = \left(\prod_{i \leq j} C_{n_i n_j}^{[ij]} + \prod_{l \leq m} \prod_k C_{n_k n_l n_m}^{[klm]} + \dots \right)$ for every $|n\rangle$ utilized in $|\Phi_p^{\text{CSF}}\rangle$ and $\tilde{\mathbf{C}}$ defines a set of correlators $\{\mathbf{C}^{[11]}, \mathbf{C}^{[12]}, \dots, \mathbf{C}^{[ij]}, \dots, \mathbf{C}^{[NM]}\}$ constituting C_n^{sa} . With the weights $S_p(\tilde{\mathbf{C}})$ from Eq. (26), we define the spin-adapted TNS ansatz as

$$|\Psi_L^{\text{sa}}\rangle = \sum_p S_p(\tilde{\mathbf{C}}) |\Phi_p^{\text{CSF}}\rangle. \quad (27)$$

The most efficient way to optimize correlators so far appeared to be the variational Monte Carlo scheme,^{34,49} for which it is useful to rewrite the expression for E_{SATNS} as

$$E_{\text{SATNS}} = \frac{\sum_r S_r(\tilde{\mathbf{C}})^2 E_r(\tilde{\mathbf{C}})}{\sum_{pq} S_p(\tilde{\mathbf{C}}) S_q(\tilde{\mathbf{C}}) \sum_n K_{pn} K_{qn}}, \quad (28)$$

where $S_r(\tilde{\mathbf{C}})^2$ is a probability distribution for energy estimators

$$E_r(\tilde{\mathbf{C}}) = \sum_s \frac{S_s(\tilde{\mathbf{C}})}{S_r(\tilde{\mathbf{C}})} \langle \Phi_s^{\text{CSF}} | H | \Phi_r^{\text{CSF}} \rangle. \quad (29)$$

Having introduced an artificial thermal energy T (measured in Hartree), the continuous variables $\tilde{\mathbf{C}}$ are sampled following a canonical ensemble with the configuration weights defined by $\exp[-E_r(\tilde{\mathbf{C}})/T]$. For higher efficiency, the parallel tempering scheme is applied³⁴ during the optimization with swap-move probabilities between two neighboring temperatures defined as

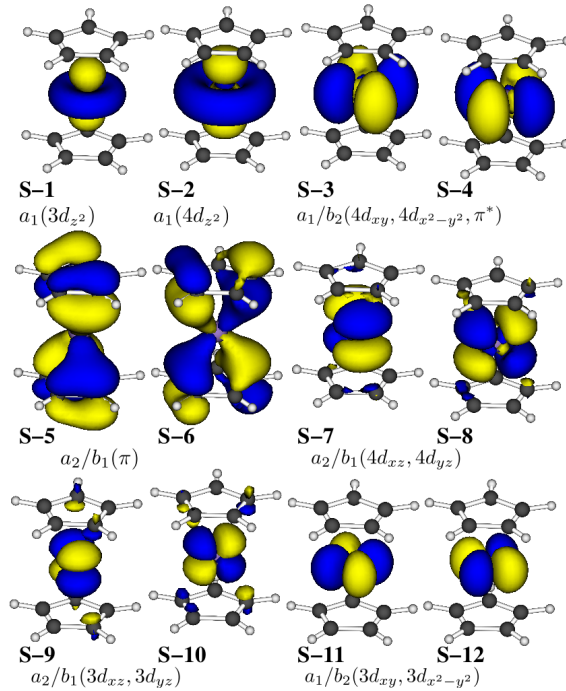
$$p((T_i, E_i) \leftrightarrow (T_{i+1}, E_{i+1})) = \min\{1, \exp(\Delta E/\Delta T)\}, \quad (30)$$

where $\Delta E = E_{i+1} - E_i$ and $\Delta T = T_{i+1}T_i/(T_i - T_{i+1})$. Each T_l in the range $[T_1, T_P]$ is defined through the formula

$$T_l = T_1 \left(\exp \frac{\ln T_P - \ln T_1}{P - 1} \right)^{l-1}, \text{ with } l = 1 \dots P. \quad (31)$$

Clearly an application of this optimization strategy is limited by the exponential scaling of the Hilbert space. Hence, it will only be feasible to work in a large CAS if not all CSFs are required so that those which hardly contribute can be omitted.

Figure 2: Natural orbitals of manganocene in the lowest-energy sextet state that constitute the active spaces in the CAS(9,12)-SCF reference reproduced from the data published in Ref. 39 (C_{2v} symmetry).

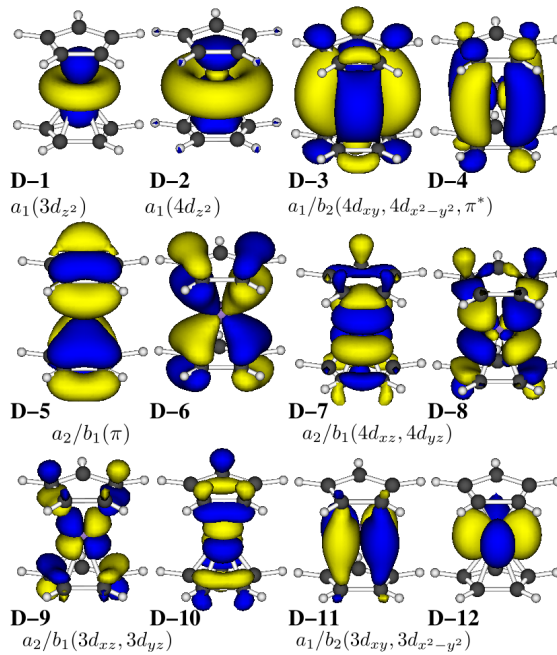


3 Computational Details

To demonstrate the efficiency of the self-adaptive scheme compared to the multi-site CGTNS approach, we consider the manganocene complex, which served as an example in our previous work.³⁹ The structures of manganocene in doublet and sextet states as well as the doublet and sextet CAS(9,12)-SCF reference energies were taken from that previous work.³⁹ In order to introduce orbital labels for the discussion below,

the converged natural orbitals from the CAS(9,12)-SCF calculation in C_{2v} symmetry reported in Ref. 39 for the sextet state (6A_1) are shown in Figure 2 and for the doublet (2A_1) in Figure 3. For the second-quantized electronic Hamiltonian, the SATNS calculations employ one- and two-electron molecular orbital integrals generated from these natural orbitals. We refer to Ref. 39 for details on how these orbitals and energies were obtained.

Figure 3: Natural orbitals for manganocene in the lowest-lying doublet state that constitute the active spaces in the CAS(9,12)-SCF reference reproduced from the data published in Ref. 39 (C_{2v} symmetry).



In our CGTNS program,³⁹ we implemented the single-orbital entropies and the self-adaptive ansatz, Ψ_n^{sa} , discussed in Sections 2.2 and 2.3, respectively. The reference values of single-orbital entropies were taken from MPS-DMRG calculations carried out with QCMAQUIS,⁵⁰ which employed the natural orbitals from the reference CAS-SCF wave functions. The number of renormalized block states in these DMRG calculations was set to 1000, while the maximum number of sweeps was limited to 20.

The parallel tempering Monte Carlo scheme described in Section 2.4 was employed for optimization of SATNS ansatz. The extension of the SATNS ansatz with a new set of correlators was made every 20 Monte Carlo steps. This, in general, appeared to be enough for reaching convergence within the active set of correlators, although a more

rigorous control for changing to the new correlator set can be based on the convergence of the energy and the single-orbital entropies. Note also that correlators at the beginning of the optimization, when SATNS ansatz lacks variational freedom, might fail to adequately describe the true wave function. Hence, the thorough relaxation of correlators may converge the ansatz to a wrong solution, which would create additional difficulties in the optimization of higher-order correlators. For the same reason, our SATNS ansatz performs quick pre-optimization (20 Monte Carlo steps) of the 2-site correlators instead of employing the fully relaxed 2-site correlators from the Ψ^{2s} ansatz (as in the case of $\Psi^{3s+[2s]}$ ansatz). However, once all necessary higher-order correlators are introduced one can perform a second optimization round. *I.e.*, the algorithm continues with a refinement of the SATNS ansatz starting over from 2-site correlators and switching to subsequent sets of correlators in the same order as it was done in the first optimization round. As will be shown in Section 4.1 this might lower the energy further. If the improvement is significant, the algorithm can continue performing optimization rounds until convergence is achieved.

4 Results

In this section, we calculate the adiabatic doublet–sextet electronic energy splitting of the manganocene spin-crossover complex with our SATNS ansatz. As can be understood from our previous results,³⁹ the electronic states of manganocene represent a challenging test for electronic structure methods in general and for CGTNS-type schemes in particular. The reference CAS(9,12)-SCF data, the data for 2- and 3-site CGTNS parameterizations (Ψ^{2s} and Ψ^{3s}), as well as for the hybrid ansatz, $\Psi^{3s+[2s]}$, were taken from the Ref. 39.

4.1 Manganocene sextet

The CAS(9,12)-SCF wave function for manganocene in its lowest-energy sextet state features a rather small variational space of 13108 ONVs that can be well approximated with the 2-site correlator ansatz.³⁹ Such an approximation eliminates 91 % of the CAS-CI variational space introducing an error of around 15 mHartree, see Table I. Unfortunately, if one employs solely 3-site correlators through the Ψ^{3s} ansatz or in a hybrid scheme together with the 2-site correlators as in the $\Psi^{3s+[2s]}$ ansatz, this does not improve the energy significantly and yields in the best case only -1542.197777 Hartree.

Together with the fact that the variational space is increased by 59 % in this case, the ansatz is rendered useless.

Table I: Electronic energies for the sextet state of manganocene calculated with various CGTNS-type parameterizations, SATNS, and CAS(9,12)-SCF.

parameterization	parameters	energy/Hartree
first optimization round		
CAS-SCF	13108	-1542.209620 ^a
Ψ_3^{sa}	4608	-1542.209585
Ψ^{3s}	20800	-1542.197777 ^a
$\Psi^{3s[2s]}$	20800	-1542.195283 ^a
Ψ^{2s}	1200	-1542.194072 ^a
second optimization round		
Ψ_3^{sa}	4608	-1542.209603

^athese electronic energies were taken from Ref. 39.

This problem is solved by the SATNS ansatz. As expected, after 20 Monte Carlo steps in the optimization of 2-site correlators, the energy of the SATNS ansatz (based solely on 2-site correlators) does not reach the minimum of a Ψ^{2s} ansatz, which is slightly lower (see Figure 4). In order to study the convergence of SATNS, we monitor the entanglement of the orbitals in Figure 5, where the reference single-orbital entropies were taken from the MPS-DMRG calculation. The reference single-orbital entropies are degenerate and have only five different values 0.0323, 0.0317, 0.0416, 0.0309, 0.0185 for sets **{S-1, S-2}**, **{S-11, S-3, S-12, S-4}**, **{S-9, S-10}**, **{S-7, S-8}**, **{S-5, S-6}**, respectively. One can see that the 2-site correlators poorly describe the entanglement between orbitals. In the region up to Monte Carlo step 20, the values of single-orbital entropies for all orbitals are far from the reference values and oscillate during the optimization. As the orbital **S-10** has the largest single-orbital entropy the SATNS scheme introduces corresponding 3-site correlators according to Eq. (19) and one observes a large energy drop, see Figure 4. Note that only the first set of 3-site correlators provides such a pronounced decrease in energy. Also, this set considerably improves the values of single-orbital entropies for almost all orbitals except for **S-5** and **S-6**. The entanglement for these orbitals approaches the reference only after the extension of the ansatz with the correlators for the orbitals **S-9** and **S-4**. For these correlator sets, one can again observe significant decreases in energy which brings the SATNS electronic energy very close to the reference value. Introducing correlators gradually for the most entangled orbitals, the SATNS manages to bypass the optimization problems observed in Ref. 39 for the $\Psi^{3s[2s]}$ and Ψ^{3s} parameterizations. In contrast to Ψ^{3s} , it reduces the

variational space by 65 %, optimizing only 4608 variational parameters at a time. The CPU time required for one Monte Carlo step in the optimization of 3-site correlators in Ψ_3^{sa} ansatz is only 1.46 times longer than the one for the Ψ^{2s} ansatz, while in the case of Ψ^{3s} and $\Psi^{3s[2s]}$ it is 4.77 times longer. If the 3-site correlators are introduced for all orbitals, the error in energy will be less than 0.1 mHartree, see Table I. In this case, the single-orbital entropies closely approach the reference values, see Figure 5. An extension of the ansatz with 4-site correlators only leads to a negligible decrease of the electronic energy, hence showing that the 2- and 3-site correlators alone are able to adequately approximate the wave function for manganocene in the sextet state.

Figure 4: Convergence behavior of the Ψ_3^{sa} , Ψ^{3s} , and $\Psi^{3s[2s]}$ parameterizations for manganocene in the lowest-lying sextet state. The data for Ψ^{2s} , Ψ^{3s} , $\Psi^{3s[2s]}$, and reference CAS(9,12)-SCF were taken from Ref. 39. Vertical gray dashed lines show the Monte Carlo steps in which new correlators were introduced. The vertical red dashed line indicates the Monte Carlo step in which the algorithm switched from 2-site to 3-site correlators.

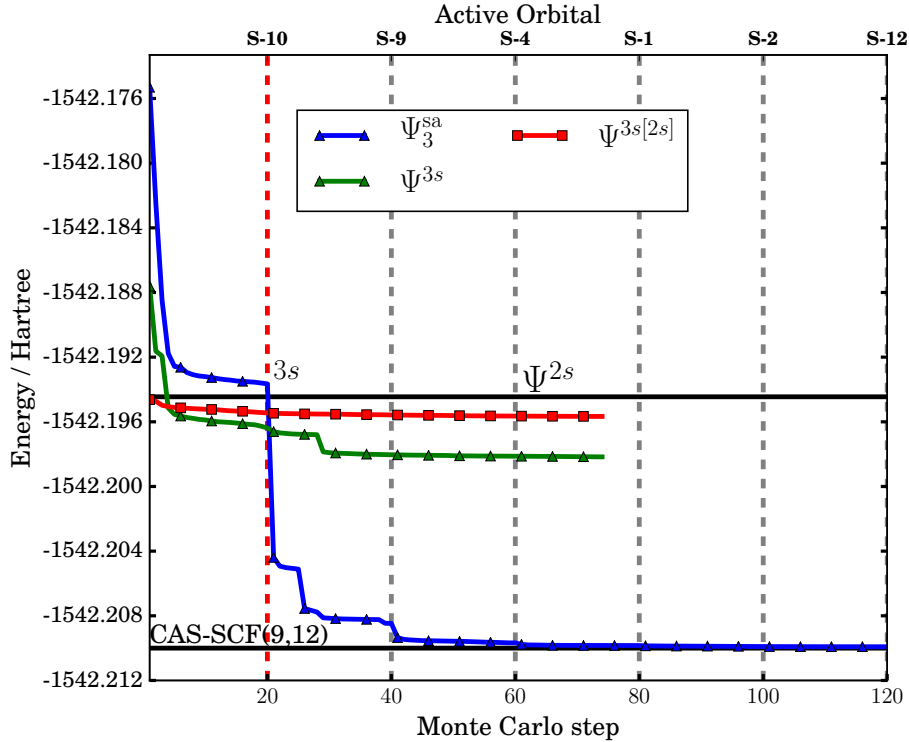
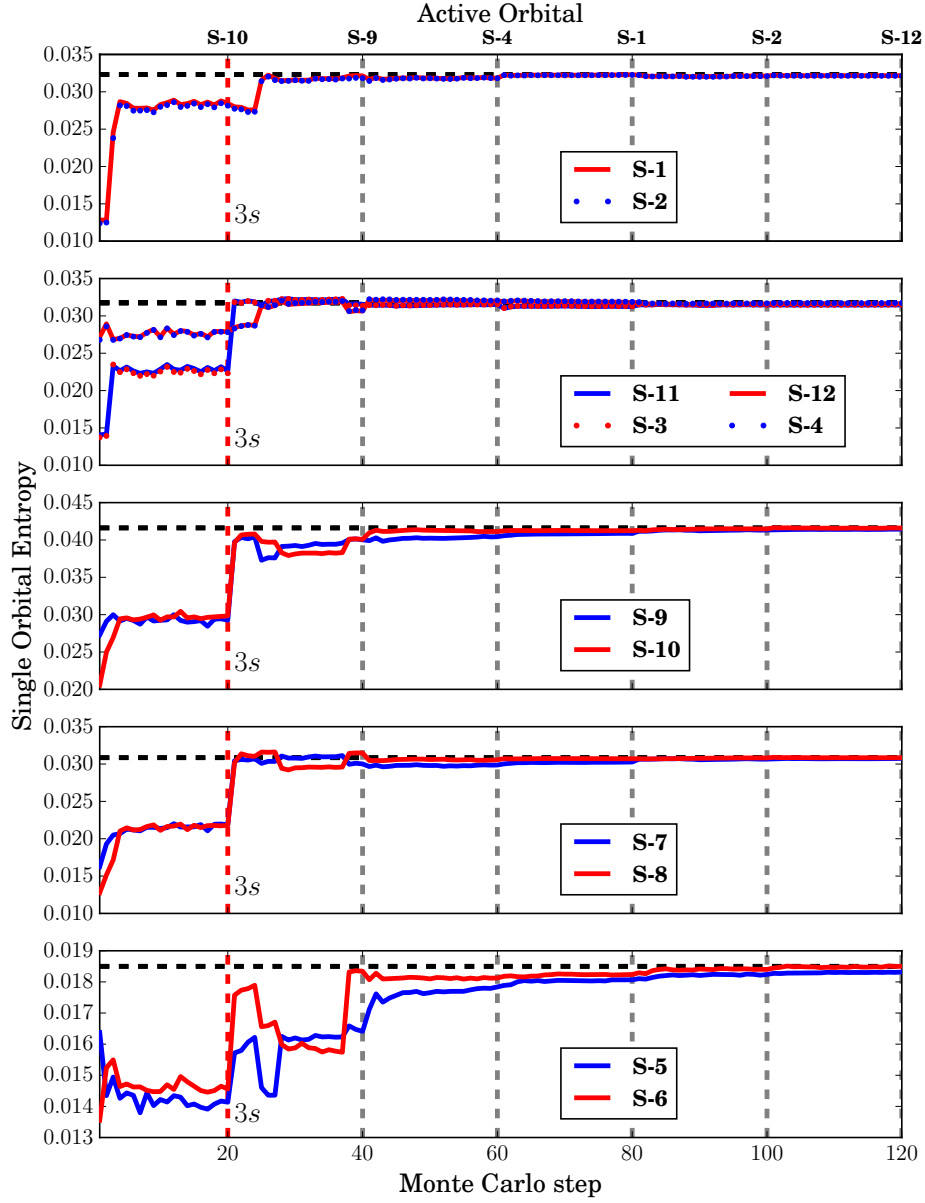


Figure 5: Convergence behavior of single-orbital entropies (manganocene in the lowest-energy sextet state) for the Ψ^{sa} ansatz. The reference values of the single-orbital entropies are taken from a MPS-DMRG calculation and shown as horizontal black dashed lines. We identify five sets, each composed of near degenerate single-orbital entropies, namely $\{\text{S-1}, \text{S-2}\}$, $\{\text{S-11}, \text{S-3}, \text{S-12}, \text{S-4}\}$, $\{\text{S-9}, \text{S-10}\}$, $\{\text{S-7}, \text{S-8}\}$, and $\{\text{S-5}, \text{S-6}\}$. Vertical gray dashed lines indicate the Monte Carlo steps in which new correlators were introduced. The vertical red dashed line shows the Monte Carlo step in which the order changed from 2-site to 3-site).



The same holds also true for the entanglement between the orbitals. Such a fast convergence of the SATNS wave function can, however, be attributed to the relatively simple entanglement pattern found for this electronic state. Note the rather small single-orbital entropies ($0 < s_i(1) < 0.1$).⁵¹ Although the 3-site-correlator SATNS ansatz Ψ_3^{sa} provides a significantly more accurate energy compared to the Ψ^{3s} ansatz, one still can improve on it by letting all correlator sets relax further in a second optimization round. This yields an electronic energy of -1542.209603 Hartree, see Table I.

4.2 Manganocene doublet

In contrast to the sextet state, the doublet state has a larger variational space of 98000 ONVs with a more complicated entanglement pattern. The single-orbital entropies for the orbitals **D-1**, **D-12**, **D-2**, **D-3**, **{D-5, D-6}**, **D-4**, **{D-10, D-9}**, **D-11**, and **{D-7, D-8}** are 0.1976, 0.1311, 0.1676, $\{0.2125, 0.2121\}$, 0.2236, $\{0.2320, 0.2316\}$, 0.2489, $\{0.0097, 0.0097\}$, respectively (the orbitals in curly brackets have near-degenerate values of single-orbital entropies). All the orbitals except **D-7** and **D-8** have moderately large single-orbital entropies ($0.1 < s_i(1) < 0.5$).⁵¹

If the CGTNS parameterizations from Section 2.1 are considered, the most accurate value of the energy is obtained with the $\Psi^{3s[2s]}$ ansatz.³⁹ Still, the error of this parameterization is half of the energy difference between the reference value and the energy of the Ψ^{2s} ansatz, while one Monte Carlo step is 4.81 times slower than one for the Ψ^{2s} ansatz. The SATNS reaches the accuracy of the $\Psi^{3s[2s]}$ ansatz after an extension with the first set of 3-site correlators for the orbital **D-11**, see Figure 6. The single-orbital entropies for all orbitals oscillate during the optimization and poorly approximate the reference wave function until the 3-site correlators are introduced, see Figure 7. For the orbitals with a high value for the single-orbital entropy, namely **D-10**, **D-9**, **D-11**, **D-4**, **D-5**, and **D-6**, the entanglement is significantly underestimated. Also the entanglement pattern for these orbitals is considerably improved with the introduction of the first 3-site correlator set. The other orbitals, however, do not experience such an improvement. Their single-orbital entropies slowly converge to the reference values with an introduction of 3-site correlators for the rest of the most entangled orbitals, namely **D-4**, **D-10**, **D-9**, **D-6**, and **D-5**. From the energy convergence shown in Figure 6, one can clearly see that these orbitals are also responsible for the major decrease of the electronic energy. With the introduction of 3-site correlators for the orbitals **D-2**, **D-12**, **D-3**, **D-7**, **D-8**, the energy slowly decreases, but does not reach the same accuracy as for the case of the sextet yielding only -1542.143410 Hartree, see Table II

and Figure 6.

Table II: Electronic energies for the doublet state of manganocene calculated with various CGTNS-type parameterizations, SATNS, and CAS(9,12)-SCF.

parameterization	parameters	energy/Hartree
first optimization round		
CAS-SCF	98060	-1542.144937 ^a
Ψ_4^{sa}	78400	-1542.144416
Ψ_3^{sa}	4608	-1542.143410
$\Psi_{3s[2s]}^{3s}$	20800	-1542.125171 ^a
Ψ^{3s}	20800	-1542.119695 ^a
Ψ^{2s}	1200	-1542.104681 ^a

^athese electronic energies were taken from Ref. 39.

The reduction in variational space achieved by the Ψ_3^{sa} ansatz is with 95% high and one Monte Carlo step in the optimization of the set of 3-site correlators is almost as fast as for the Ψ^{2s} ansatz, see Table II. Extending the self-adaptive ansatz toward 4-site correlators one observes a nonnegligible drop in energy, which shows the importance of 4-site correlators for the wave function in contrast to the sextet state. One Monte Carlo step in the optimization of the 4-site correlators in the Ψ_4^{sa} ansatz is 3.87 times slower in comparison to the Ψ^{2s} ansatz. After the introduction of the 4-site correlators for all orbitals the energy for the doublet state becomes -1542.144416 Hartree, for which, however, 80 % of the CAS-CI variational space is required.

A problem occurs for the entanglement description of orbital **D-11**. The corresponding single-orbital entropy, after reaching the reference value at Monte Carlo step 100, continues to grow and at Monte Carlo step 320 it is slightly overestimated. A possible reason might be an insufficient entanglement description in the SATNS ansatz at the beginning of the optimization: at Monte Carlo step 40, the 3-site correlators were introduced for the **D-4** orbital, as it had the second largest single-orbital entropy in that step. But the better choice should have been made in favor of the **D-10** orbital since it has the second largest single-orbital entropy according to the reference wave function and the SATNS at later stages of an optimization. If such issues are not properly resolved in not fully optimized SATNS wave functions, parallel or simultaneous optimization strategies may be considered.

Figure 6: Convergence behavior of the Ψ_4^{sa} , Ψ^{3s} , and $\Psi^{3s[2s]}$ parameterizations for manganocene in the doublet state. The data for Ψ^{2s} , Ψ^{3s} , $\Psi^{3s[2s]}$, and reference CAS(9,12)-SCF were taken from Ref. 39. Vertical gray dashed lines show the Monte Carlo steps where new correlators are introduced. Vertical red dashed lines show the Monte Carlo steps where the order of new correlators changes (*e.g.*, from 2-site to 3-site).

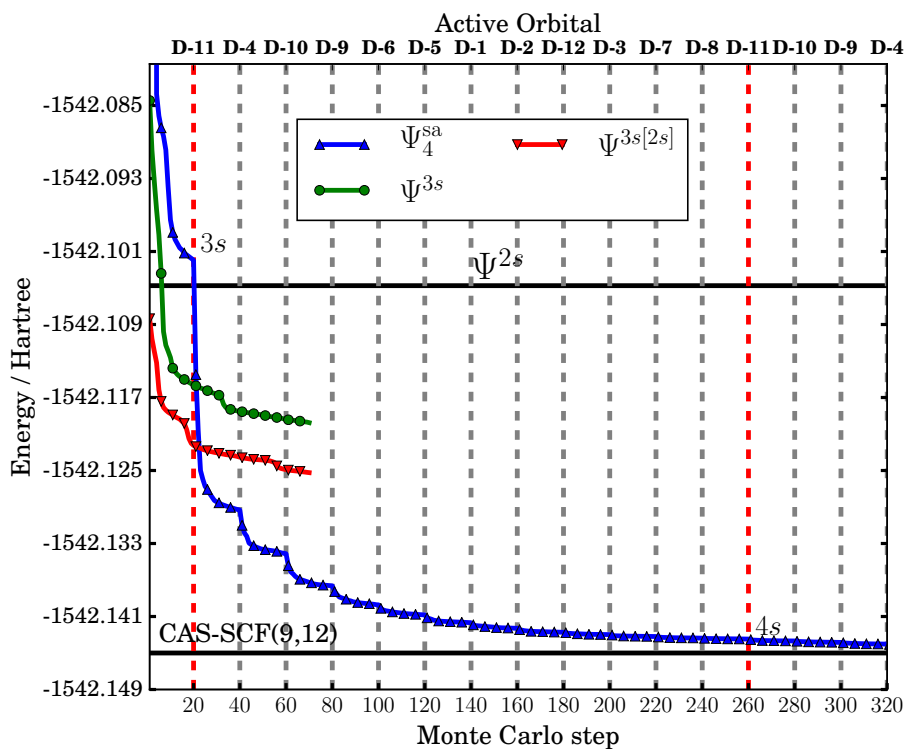
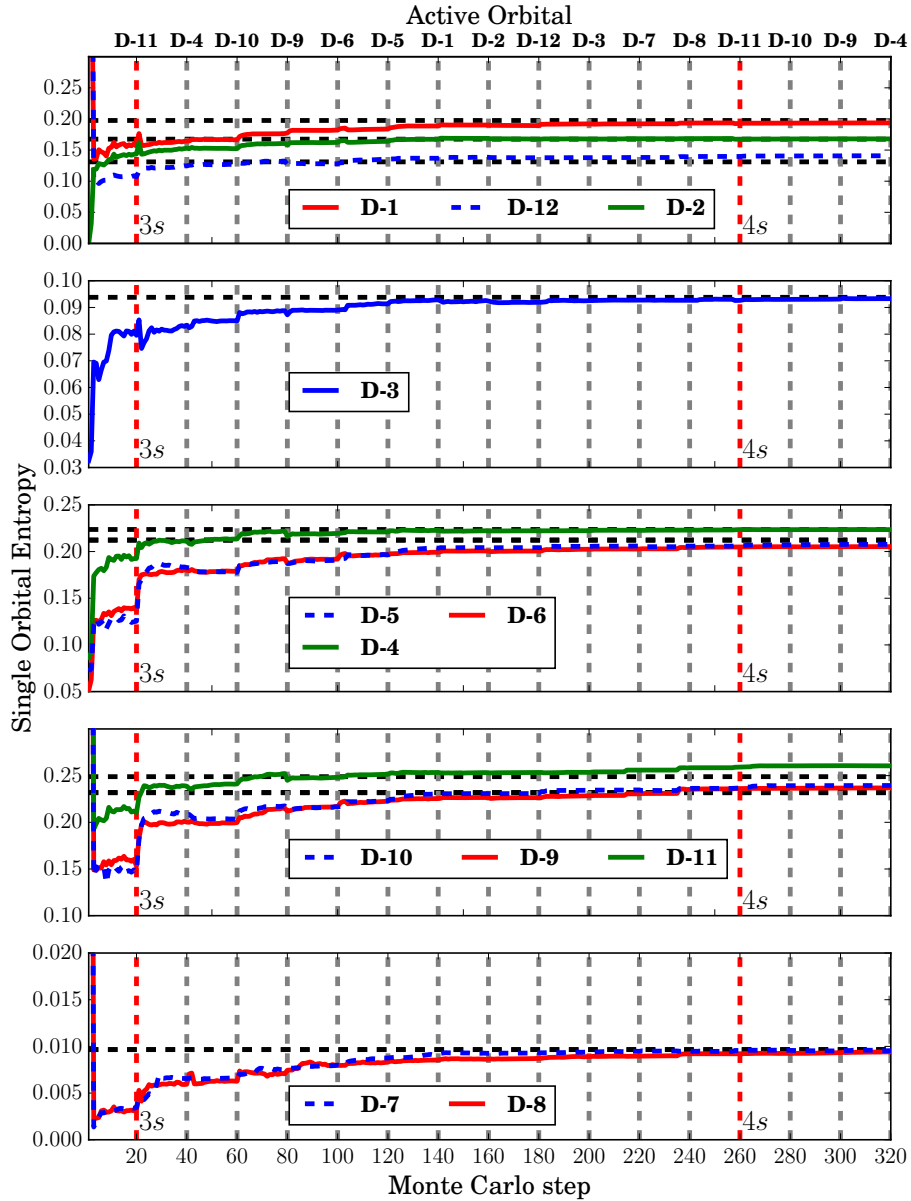


Figure 7: Convergence behavior of single-orbital entropies (manganocene in the doublet state) for the self-adaptive Ψ^{sa} ansatz. The reference values of the single-orbital entropies are taken from a MPS-DMRG calculation are shown as horizontal black dashed lines. For the better readability the data were split into 5 sets: $\{\text{D-1}, \text{D-12}, \text{D-2}\}$, $\{\text{D-3}\}$, $\{\text{D-5}, \text{D-6}, \text{D-4}\}$, $\{\text{D-10}, \text{D-9}, \text{D-11}\}$, and $\{\text{D-7}, \text{D-8}\}$. Some of the single-orbital entropies form near degenerate sets, namely $\{\text{D-5}, \text{D-6}\}$, $\{\text{D-10}, \text{D-9}\}$, and $\{\text{D-7}, \text{D-8}\}$. Vertical gray dashed lines indicate the Monte Carlo steps in which new correlators were introduced. Vertical red dashed lines point to those Monte Carlo steps in which the order of new correlators changes (*e.g.*, from 2-site to 3-site).



4.3 Sextet–doublet energy splitting

To demonstrate the accuracy of our self-adaptive tensor network approach for the more relevant relative energies, we summarize the results of CGTNS parameterizations from our previous work.³⁹ The worst approximation for the energy splitting is obtained with the Ψ^{2s} ansatz, which yields -56.09 kcal/mol, see Table III. 3-site correlators reduce the error relative to the CAS(9,12)-SCF reference from 16.5 to 8.41 kcal/mol. If 2-site correlators are combined with 3-site correlators in the hybrid $\Psi^{3s[2s]}$ scheme, the error is decreased further to 3.41 kcal/mol. The self-adaptive ansatz dramatically improves on those results: already a SATNS parameterization with correlators up to only third order reduces the error to 0.94 kcal/mol. Employing Ψ_3^{sa} for the sextet and Ψ_4^{sa} for the doublet yields an error of 0.31 kcal/mol.

Table III: The doublet–sextet energy differences in kcal/mol for manganocene calculated with various CGTNS parameterizations and CAS(9,12)-SCF.

parameterization	$E[{}^6A_1] - E[{}^2A_1]$
6A_1	2A_1 kcal/mol
CAS-SCF	-40.59 ^a
Ψ_3^{sa}	Ψ_4^{sa} -40.90
Ψ_3^{sa}	-41.53
$\Psi^{3s[2s]}$	-44.00 ^a
Ψ^{3s}	-49.00 ^a
Ψ^{2s}	-56.09 ^a

^ataken from Ref. 39.

5 Conclusions

As the order of correlators is increased in the L -site CGTNS scheme, the fast growth of the variational space is a major problem. Moreover, the higher-order correlators make the optimization procedure much more involved. Here, we developed a self-adaptive strategy which overcomes these problems. Our SATNS strategy is based on the evaluation of single-orbital entropies, which has been introduced and implemented in this work for CGTNS-type parameterizations. The SATNS ansatz starts with the optimization of 2-site correlators. Then, based on single-orbital entropies it gradually extends an ansatz with higher-order correlators for the most entangled orbitals. Thereby, a selective optimization rather than an optimization of all higher-order correlators is

achieved. Our manganocene case study showed that the SATNS is able to systematically improve the accuracy employing only a small part of the variational space arising from the complete set of correlators of a certain order. The Ψ_3^{sa} scheme achieves an accuracy with an error of about one kcal/mol, while about 65 % of the variational space was reduced in the case of the sextet and 95 % for the doublet. Various aspects of the SATNS parametrization should be studied in future work, of which excited electronic states and gradients are two examples.

6 Acknowledgment

This work was supported by ETH Zurich (ETH Fellowship FEL-27 14-1) and by the Schweizerischer Nationalfonds (Project No. SNF 200020.169120).

References

- [1] Steven R. White. Density matrix formulation for quantum renormalization groups. *Phys. Rev. Lett.*, **69** (1992) 2863.
- [2] Ulrich Schollwöck. The density-matrix renormalization group in the age of matrix product states. *Ann. Phys.*, **326** (2011) 96–192.
- [3] Ö. Legeza, R.M. Noack, J. Sólyom, L. Tincani. Applications of Quantum Information in the Density-Matrix Renormalization Group. *Lect. Notes Phys.*, **739** (2008) 653–664.
- [4] G. K.-L. Chan, J. J. Dorando, D. Ghosh, J. Hachmann, E. Neuscamman, H. Wang, T. Yanai. An Introduction to the Density Matrix Renormalization Group Ansatz in Quantum Chemistry. *Prog. Theor. Chem. Phys.*, **18** (2008) 49–65.
- [5] Garnet Kin-Lic Chan, Dominika Zgid. The Density Matrix Renormalization Group in Quantum Chemistry. *Annu. Rep. Comput. Chem.*, **5** (2009) 149–162.
- [6] Konrad Heinrich Marti, Markus Reiher. The Density Matrix Renormalization Group Algorithm in Quantum Chemistry. *Z. Phys. Chem.*, **224** (2010) 583–599.
- [7] Konrad H. Marti, Markus Reiher. New electron correlation theories for transition metal chemistry. *Phys. Chem. Chem. Phys.*, **13** (2011) 6750–6759.

- [8] Garnet Kin-Lic Chan, Sandeep Sharma. The Density Matrix Renormalization Group in Chemistry. *Ann. Rev. Phys. Chem.*, **62** (2011) 465.
- [9] Wouters, Sebastian, Van Neck, Dimitri. The density matrix renormalization group for ab initio quantum chemistry. *Eur. Phys. J. D*, **68**(9) (2014) 272.
- [10] Yuki Kurashige. Multireference Electron Correlation Methods with Density Matrix Renormalisation Group Reference Functions. *Mol. Phys.*, **112**(11) (2014) 1485–1494.
- [11] Takeshi Yanai, Yuki Kurashige, Wataru Mizukami, Jakub Chalupský, Tran Nguyen Lan, Masaaki Saitow. Density matrix renormalization group for ab initio calculations and associated dynamic correlation methods: A review of theory and applications. *Int. J. Quantum Chem.*, **115**(5) (2015) 283–299.
- [12] Szilárd Szalay, Max Pfeffer, Valentin Murg, Gergely Barcza, Frank Verstraete, Reinhold Schneider, Örs Legeza. Tensor product methods and entanglement optimization for ab initio quantum chemistry. *Int. J. Quantum Chem.*, **115**(19) (2015) 1342–1391.
- [13] Konrad H. Marti, Irina Malkin Ondik, Gerrit Moritz, Markus Reiher. Density matrix renormalization group calculations on relative energies of transition metal complexes and clusters. *J. Chem. Phys.*, **128** (2008) 014104.
- [14] Katharina Boguslawski, Konrad H. Marti, Örs Legeza, Markus Reiher. Accurate ab initio spin densities. *J. Chem. Theory Comput.*, **8** (2012) 1970–1982.
- [15] Yuki Kurashige, Garnet Kin-Lic Chan, Takeshi Yanai. Entangled quantum electronic wavefunctions of the Mn_4CaO_5 cluster in photosystem II. *Nature Chem.*, **5** (2013) 1755–4330.
- [16] Sandeep Sharma, Kantharuban Sivalingam, Frank Neese, Garnet Kin-Lic Chan. Low-energy spectrum of iron-sulfur clusters directly from many-particle quantum mechanics. *Nature Chem.*, **6** (2014) 927–933.
- [17] Quan Manh Phung, Sebastian Wouters, Kristine Pierloot. Cumulant approximated second-order perturbation theory based on the density matrix renormalization group for transition metal complexes: A benchmark study. *Journal of Chemical Theory and Computation*, **12** (2016) 4352–4361.
- [18] S. Östlund, S. Rommer. Thermodynamic limit of density-matrix renormalization. *Phys. Rev. Lett.*, **75** (1995) 3537–40.

- [19] Wolfgang Hackbusch. *Tensor Spaces and Numerical Tensor Calculus*. Springer, Leipzig, 2012.
- [20] Garnet Kin-Lic Chan, Martin Head-Gordon. Highly correlated calculations with a polynomial cost algorithm: A study of the density matrix renormalization group. *J.Chem. Phys.*, **116**(11) (2002) 4462–4476.
- [21] Ö. Legeza, J. Sólyom. Optimizing the density-matrix renormalization group method using quantum information entropy. *Phys. Rev. B*, **68** (2003) 195116.
- [22] Gerrit Moritz, Bernd Artur Hess, Markus Reiher. Convergence behavior of the density-matrix renormalization group algorithm for optimized orbital orderings. *J. Chem. Phys.*, **122**(2) (2005) 024107.
- [23] G. Barcza, Ö. Legeza, K. H. Marti, M. Reiher. Quantum-information analysis of electronic states of different molecular structures. *Phys. Rev. A*, **83** (2011) 012508.
- [24] C. Krumnow, L. Veis, Ö. Legeza, J. Eisert. Fermionic orbital optimization in tensor network states. *Phys. Rev. Lett.*, **117** (2016) 210402.
- [25] Frank Verstraete, J. Ignacio Cirac. Renormalization algorithms for quantum-many body systems in two and higher dimensions. *arXiv:cond-mat/0407066*, 2004.
- [26] Y.-Y Shi, L.-M. Duan, G. Vidal. Classical simulation of quantum many-body systems with a tree tensor network. *Phys. Rev.*, **74** (2006) 022320.
- [27] L. Tagliacozzo, G. Evenbly, G. Vidal. Simulation of two-dimensional quantum systems using a tree tensor network that exploits the entropic area law. *Phys. Rev. B*, **80** (2009) 235127.
- [28] Philippe Corboz, Guifré Vidal. Fermionic multiscale entanglement renormalization ansatz. *Phys. Rev. B*, **80** (2009) 165129.
- [29] V. Murg, F. Verstraete, Ö. Legeza, R. M. Noack. Simulating strongly correlated quantum systems with tree tensor networks. *Phys. Rev. B*, **82** (2010) 205105.
- [30] Naoki Nakatani, Garnet Kin-Lic Chan. Efficient tree tensor network states (TTNS) for quantum chemistry: Generalizations of the density matrix renormalization group algorithm. *J. Chem. Phys.*, **138** (2013) 134113.
- [31] Valentin Murg, Frank Verstraete, Reinhold Schneider, Peter Nagy, Örs Legeza. Tree tensor network state with variable tensor order: An efficient multireference method for strongly correlated systems. *J. Chem. Theory Comput.*, **11** (2015) 1027.

- [32] G. Evenbly, G. Vidal. Class of highly entangled many-body states that can be efficiently simulated. *Phys. Rev. Lett.*, **112** (2014) 240502.
- [33] Nicholas J. Mayhall. Using higher-order singular value decomposition to define weakly coupled and strongly correlated cluster states: the n-body Tucker approximation. *J. Chem. Theor. Comput.*, p. DOI: 10.1021/acs.jctc.7b00696.
- [34] Konrad H. Marti, Bela Bauer, Markus Reiher, Matthias Troyer, Frank Verstraete. Complete-graph tensor network states: a new fermionic wave function ansatz for molecules. *New J. Phys.*, **12** (2010) 103008.
- [35] Andrej Gendiar, Tomotoshi Nishino. Latent heat calculation of three-dimensional $q = 3, 4$, and 5 potts models by the tensor product variational approach. *Phys. Rev. E*, **65** (2002) 046702.
- [36] Andrej Gendiar, Nobuya Maeshima, Tomotoshi Nishino. Stable optimization of a tensor product variational state. *Prog. Theor. Phys.*, **110** (2003) 691–699.
- [37] Fabio Mezzacapo, Norbert Schuch, Massimo Boninsegni, J. Ignacio Cirac. Ground-state properties of quantum many-body systems: entangled-plaquette states and variational Monte-Carlo. *New J. Phys.*, **11** (2009) 083026.
- [38] Hitesh J. Changlani, Jesse M. Kinder, C. J. Umrigar, Garnet Kin-Lic Chan. Approximating strongly correlated wave functions with correlator product states. *Phys. Rev. B*, **80** (2009) 245116.
- [39] Arseny Kovyrshin, Markus Reiher. Tensor network states with three-site correlators. *New J. Phys.*, **18** (2016) 113001.
- [40] Ö. Legeza, J. Sólyom. Quantum data compression, quantum information generation, and the density-matrix renormalization-group method. *Phys. Rev. B*, **70** (2004) 205118.
- [41] Jörg Rissler, Reinhard M. Noack, Steven R. White. Measuring orbital interaction using quantum information theory. *Chem. Phys.*, **323** (2006) 519–531.
- [42] Eric Neuscamman, Hitesh Changlani, Jesse Kinder, Garnet Kin-Lic Chan. Non-stochastic algorithms for jastrow-slater and correlator product state wave functions. *Phys. Rev. B*, **84** (2011) 205132.
- [43] J. C. Greer. Estimating full configuration interaction limits from a monte carlo selection of the expansion space. *J. Chem. Phys.*, **103** (1995) 1821–1828.

- [44] George H. Booth, Alex J. W. Thom, Ali Alavi. Fermion monte carlo without fixed nodes: A game of life, death, and annihilation in slater determinant space. *J. Chem. Phys.*, **131** (2009) 054106.
- [45] Francesco Aquilante, Jochen Autschbach, Rebecca K. Carlson, Liviu F. Chibotaru, Mickaël G. Delcey, Luca De Vico, Ignacio Fdez. Galván, Nicolas Ferré, Luis Manuel Frutos, Laura Gagliardi, Marco Garavelli, Angelo Giussani, Chad E. Hoyer, Giovanni Li Manni, Hans Lischka, Dongxia Ma, Per Åke Malmqvist, Thomas Müller, Artur Nenov, Massimo Olivucci, Thomas Bondo Pedersen, Daoling Peng, Felix Plasser, Ben Pritchard, Markus Reiher, Ivan Rivalta, Igor Schapiro, Javier Segarra-Martí, Michael Stenrup, Donald G. Truhlar, Liviu Ungur, Alessio Valentini, Steven Vancoillie, Valera Veryazov, Victor P. Vysotskiy, Oliver Weingart, Felipe Zapata, Roland Lindh. Molcas 8: New capabilities for multiconfigurational quantum chemical calculations across the periodic table. *J. Comput. Chem.*, **37** (2016) 506–541.
- [46] Richard P. Stanley. *Enumerative Combinatorics*. Cambridge University Press, New York, 1997.
- [47] Jennifer J. Quinn Arthur T. Benjamin. *Proofs that Really Count: The Art of Combinatorial Proof*. The Mathematical Association of America, Washington, 2003.
- [48] Katharina Boguslawski, Pawel Tecmer. Orbital entanglement in quantum chemistry. *Int. J. Quantum Chem.*, **115** (2015) 1289–1295.
- [49] A. W. Sandvik, G. Vidal. Variational Quantum Monte Carlo Simulations with Tensor-Network States. *Phys. Rev. Lett.*, **99** (2007) 220602.
- [50] Sebastian Keller, Markus Reiher. Spin-adapted matrix product states and operators. *J. Chem. Phys.*, **144** (2016) 134101.
- [51] Katharina Boguslawski, Pawel Tecmer, Örs Legeza, Markus Reiher. Entanglement measures for single- and multireference correlation effects. *J. Phys. Chem. Lett.*, **3** (2012) 3129–3135.